PAPER

Antimony oxide nanostructures in the monolayer limit: self-assembly of van der Waals-bonded molecular building blocks

To cite this article: Tobias Märkl et al 2021 Nanotechnology 32 125701

View the <u>article online</u> for updates and enhancements.



Nanotechnology 32 (2021) 125701 (8pp)

Antimony oxide nanostructures in the monolayer limit: self-assembly of van der Waals-bonded molecular building blocks

Tobias Märkl¹, Sara Salehitaleghani¹, Maxime Le Ster¹, Pawel J Kowalczyk², Xiaoxiong Wang³, Peng Wang⁴, Matthew Snyder⁵, Guang Bian⁵, Tai-Chang Chiang⁶ and Simon A Brown¹

E-mail: simon.brown@canterbury.ac.nz

Received 30 September 2020 Accepted for publication 3 December 2020 Published 30 December 2020



Abstract

Antimony oxide nanostructures have been identified as candidates for a range of electronic and optoelectronic applications. Here we demonstrate the growth of 2-dimensional antimony oxide nanostructures on various substrates, including highly oriented pyrolytic graphite (HOPG), MoS_2 and α -Bi(110) nanoislands. Using scanning tunneling microscopy (STM) we show that the nanostructures formed are exclusively highly crystalline α -Sb₂O₃(111) monolayers with a lattice constant of 796 pm \pm 7 pm. The nanostructures are triangular with lateral dimensions of up to \sim 30 nm. Even though elemental antimony nanostructures are grown simultaneously mixed phases are not observed and both materials exhibit their own distinct growth modes. Moiré patterns are also observed and simulated, allowing confirmation of the atomic unit cell and an understanding of the orientation of the Sb₂O₃ structures with respect to the supporting materials. As in the bulk, the Sb₂O₃ nanostructures are formed from Sb₄O₆ molecules that are weakly interacting through van der Waals forces. This allows physical modification of the nanostructures with the STM tip. Scanning tunnelling spectroscopy reveals a wide band gap of at least 3.5 eV. Finally, we show that possible alternative structures that have unit cells comparable to those observed can be excluded based on our DFT calculations. The considered structures are a 2×2 reconstruction of β -Sb with one vacancy per unit cell and a van der Waals solid composed of Sb₄ clusters. Previous reports have predominantly demonstrated Sb₂O₃ structures with much larger thicknesses.

Supplementary material for this article is available online

Keywords: antimony, antimony oxide, antimony allotropes, 2-dimensional inorganic molecular crystals, van der Waals heterostructures, reconstructed structures

(Some figures may appear in colour only in the online journal)

¹ The MacDiarmid Institute for Advanced Materials and Nanotechnology, School of Physical and Chemical Sciences, University of Canterbury, Christchurch, New Zealand

² Department of Solid State Physics, Faculty of Physics and Applied Informatics, University of Lodz, Lodz, Poland

³ College of Science, Nanjing University of Science and Technology, Nanjing 210094, People's Republic of China

⁴ College of Electronic Communication and Physics, Shandong University of Science and Technology, Qingdao 266590, People's Republic of China

⁵ Department of Physics and Astronomy, University of Missouri, Columbia, MO 65211, United States of America

⁶ Department of Physics, University of Illinois at Urbana-Champaign, 1110 West Green Street, Urbana, IL 61801-3080, United States of America

1. Introduction

The emergence of two-dimensional materials as a key focus for modern materials science is driven both by potential applications and novel science. Potential application spaces include nano-electronics (opto-)electronics, catalysis and electrochemistry [1–3]. The vast potential is in no small part a consequence of the weak van der Waals (vdW) interactions between layered 2D materials, where the vdW interaction largely preserves the individual properties of the layers and thereby allows engineering of the properties of heterostructures [4].

Recently, it has been recognized that the same principles might be used for the construction of new 2D materials that are themselves comprised of vdW-bonded molecular (0D) building blocks. In particular, small inorganic molecules are promising since electronic transport via quantum tunneling and flexibility in the design of the building blocks might allow engineering of materials with unique and customized properties [5]. Among these materials, antimony trioxide (Sb₂O₃) has been identified as a semiconductor that is particularly promising for electronic or optoelectronic applications due to its wide band gap ($\geq 3.3 \text{ eV}$) [6–9].

The so-called α -phase of Sb_2O_3 is the most stable at low-temperature [9] and consists of Sb_4O_6 molecules (sometimes called 'cages') in which the four Sb atoms occupy the vertices of a tetrahedron and the six oxygen atoms bulge slightly outward from the edges (see figure 1(a)). Bulk α -Sb₂O₃ is a wide band gap semiconductor with a cubic crystal structure consisting of an alternating arrangement of these cages (figure 1(b)).

The fabrication of α -Sb₂O₃ thin films has only recently been reported [5, 11–14]. Lateral sizes up to a few tens of microns were achieved but the observed structures were typically relatively thick (multilayers with up to 80 nm thickness [5]) and structures in the single to few-monolayer regime were only rarely observed [5, 11, 12]. Several different approaches to growth have been explored, and it was reported that a passivator was required to prevent the heterophase nucleation i.e. in order to ensure growth of the α -phase in preference to other phases of the oxide [5]. Growth of a single phase without resort to a passivator, and consistent growth of structures with a single thickness (especially single monolayers), are remaining unsolved challenges.

Here we report the growth of monolayer α -Sb₂O₃(111) nanostructures alongside 2D α - and β -antimonene layers on various supporting substrates. We report a remarkable growth mode in which Sb and Sb₂O₃ structures are formed simultaneously without significant intermixing. Scanning tunneling microscopy (STM) and spectroscopy (STS) was used to reveal the 2D crystal structure, moiré patterns (MPs) and the band gap of the nanostructures. Our experimental results are further supported by band structure calculations which also allow possible alternative explanations using 2D structures based on pure Sb to be discarded.

2. Methods

We present here results obtained using highly-oriented pyrolithic graphite (grade-1 from SPI supplies) (HOPG) as a substrate, but essentially identical structures were observed for growth on MoS2. The HOPG was cleaved, immediately transferred to our ultra-high vacuum (UHV) system and degassed for 16 h at 773 K. Samples were then prepared by first depositing ~1.2 ML of Bi (99.999%) from a Knudsen cell (T = 723 K) onto the substrate, which was held at room temperature, followed by ~ 0.6 ML of Sb (99.999%, crucible at 574 K during deposition). It is likely the Sb source is oxidized when the UHV chamber is vented providing a source of Sb₄O₆—see discussion below. Using an Omicron VT AFM/STM ($P \le 5 \times 10^{-10}$ mbar) and Pt/Ir tips we carried out imaging and spectroscopy (STS) experiments at 295 and 50 K. Standard lock-in methods were used for STS, with modulation amplitudes of 20 mV (RMS) at a frequency of 2.71 kHz.

The lattice parameters as well as MP characteristics (wavelengths and angles relative to crystallographic axes) were determined using 2D fast Fourier transforms (FFTs) of topography and tunneling current maps. Wherever possible, the lattice parameters and FFTs were calibrated using atomically resolved HOPG images obtained using the same tips. Moiré patterns were modelled using a previously reported simple superposition approach [15] and using analytic formulae [16]. Atomic structure images were rendered using Vesta [17].

Density Functional Theory (DFT) calculations for Sb_2O_3 , Sb_4 and β -Sb were carried out in the framework of the generalized gradient approximation using the Vienna Ab initio Simulation Package [18]. $11 \times 11 \times 11$ and $11 \times 11 \times 1$ Monkhorst–Packk-point meshes were used for bulk and monolayer calculations, respectively. All calculations were performed with a plane-wave cutoff of $400 \, \text{eV}$.

3. Experimental results

3.1. Morphology

As has been described previously [19] typical Sb/Bi/HOPG samples consist of flat bismuth islands [20–23] on which the antimony forms additional layers with at least two different crystal structures. As shown schematically in figure 1(e) we routinely observe 2 ML α -Sb and 1 ML β -Sb structures on α -Bi island bases [19]. The bismuth islands are important in providing nucleation sites for the growth of 2-dimensional Sb layers which would otherwise grow with a 3-dimensional morphology (see [24] and references therein). The arrows in figure 1(d) indicate previously unobserved triangular structures with subnanometer thicknesses. We will show in the following that these structures are composed of Sb₂O₃.

Most of the triangular structures reside on HOPG. Triangular structures were also found (although less frequently)

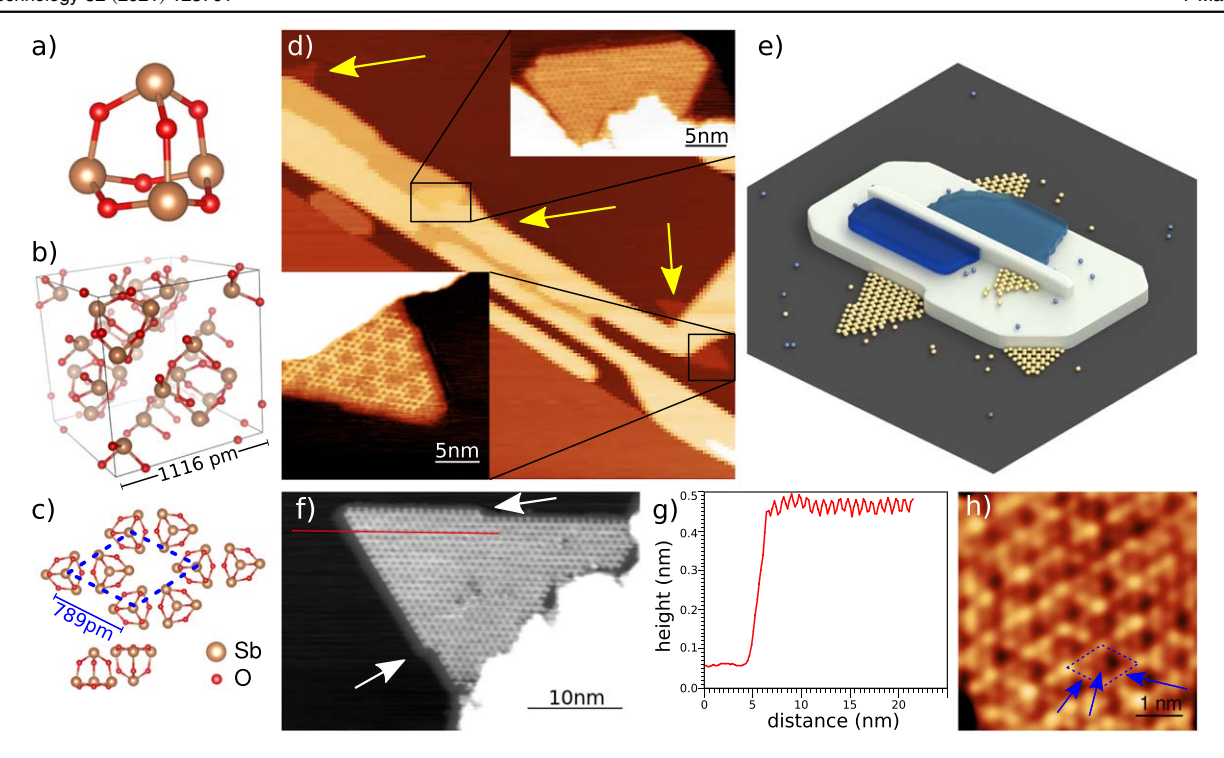


Figure 1. (a) Sb_4O_6 molecule, (b) cubic crystal structure of α - Sb_2O_3 with a lattice constant of 1116 pm [10], (c) schematic top and side view of the structure of a monolayer of the α - Sb_2O_3 (111) plane, one unit cell is indicated by a blue rhombus. The in-plane lattice constant is equal to half the face diagonal of the bulk structure in (b) (789 pm = 1116 pm/ $\sqrt{2}$). (d) General occurrence of triangular structures on Sb/Bi/HOPG samples. Yellow arrows indicate several of them attached to the Bi islands. Two insets show detailed views of triangular structures, the lower one exhibits an additional moiré pattern. (e) Schematic drawing to illustrate the growth and phase separation. Bi islands (white) on HOPG (dark gray) host 2 ML α -Sb (dark blue) and 1 ML β -Sb (light blue) on top while the triangular structures (yellow) can be found mostly around the edges. (f) A triangular structure on Bi, white arrows highlight kinks along the edges. A height profile along the red line is shown in (g). (h) Close-up scan (filtered) showing atomic resolution with additional protrusions (blue arrows) on the edges of and inside the unit cell which is represented by a blue rhombus as in (c).

on top of the Bi islands (figure 1(d), inset), regardless of the Bi thickness. The appearance of the triangular structures is clearly different from all other Bi and Sb phases that exist on this sample so that they can be reliably distinguished. In particular, there is no risk of confusing them with a Bi monolayer [25], 2 ML α -Sb, or 1 ML β -Sb [19]. In all cases the triangular structures were found to be attached to other (pre-existing) structures including edges of α -Bi or α -Sb layers (but not HOPG step edges). Unattached triangular structures are not observed either on the HOPG substrate, or on top of any of the other crystalline Bi or Sb layers. The triangular structures are absent in Bi/HOPG samples, and occur only after Sb deposition. Figure 1(e) shows a schematic overview of the growth of the triangular structures.

The triangular structures are clearly crystalline with a threefold rotational symmetry, as shown in figure 1. Moreover, a surprisingly large spatial period is immediately obvious (figures 1(d), (f), and (h)). The periodicity is measured from FFTs (see Methods and supplementary information (available online at stacks.iop.org/NANO/32/125701/mmedia)) and is found to be 800 pm \pm 10 pm which is very close to twice the lattice constant of β -Sb [19], but also very close to that of the (111) plane of bulk α -Sb₂O₃, as shown in figure 1(c).

The triangular structures are only minimally truncated, and their principal crystallographic axes are aligned with the long edges which are exclusively zig–zag type edges (figures 1(d), (f)). We do not observe any other type of facet, and the edges are defect-free apart from occasional kinks of size equal to one lattice constant in the directions both parallel and perpendicular to the edge i.e. $\sim\!800\,\mathrm{pm}$ (arrowed in figure 1(f)). We further investigate the termination of the edges, including a comparison of the experimental results with the edge configurations of model $\alpha\text{-Sb}_2\mathrm{O}_3(111)$ structures, in SI section 1. We find that an unusually open zig–zag edge provides the best match with the data.

The atomic contrast in STM images was found to vary with tip conditions, but not with bias. Typically the structure appears as bright (i.e. higher) rings with round holes (e.g. figure 1(f)) but improved spatial resolution reveals further detail at the edges and corners of the rhombohedral unit cell as shown in figure 1(h). Overall, these observations allow us to interpret the atomic scale contrast as arising from the geometric structure and not from electronic effects. We can therefore exclude charge density waves or other electronic standing waves, because the contrast is independent of bias and the kink width reflects the size of one building block.

The thickness of the triangular structures was consistently found to be uniform across the entire structure, with no evidence for steps. Apparent heights between 250 and 450 pm (e.g. figure 1(g)) were measured, depending on tip and tunneling conditions. Since steps in height profiles were

never observed we conclude that all structures comprise a single monolayer.

The triangular structures were found to be rather delicate. Repeated scanning caused them to detach from, or move along the edge of, the Bi islands, and sometimes even to break up into smaller parts. Supplementary figure S2 shows a sequence of images of a triangular structure that was damaged by the tip. In subsequent scans one of the fragments was moved by the tip along the edge of the triangular structure. The fragment then merged with the original structure without formation of any obvious defect or grain boundary. In contrast, none of the other layers (Bi, Sb or the substrate) was modified by the tip when subjected to the same tunneling conditions. This suggests that the bonding within the triangular structures is significantly weaker than in the pure Bi and Sb structures, but that the bonds are strong enough to be reformed and to ensure epitaxy between the fragments of the reformed structure. Further evidence for relatively strong bonding is provided by the results of annealing the structures: after twice annealing at 95 °C for two hours we still found triangular structures without any signs of damage or degradation.

3.2. Moiré patterns

Some of the triangular structures exhibit a clear height modulation and we show below that it is a moiré pattern, formed due to interference of the lattices of the triangular structure and the underlying HOPG. Figure 2(a) shows one example of such a modulation: in addition to the $\sim\!800\,\mathrm{pm}$ lattice constant a regular hexagonal array of depressions in the triangular structure can be observed with a much larger period. In this case the period is $\sim\!2.5\,\mathrm{nm}$ and the high symmetry directions of this superlattice are aligned with the atomic lattice (within an uncertainty of $\sim\!5^\circ$).

In this particular example we also obtained atomic resolution images of neighboring regions of the substrate (not shown). We were thus able to measure the twist angle θ between the $\langle 10 \rangle$ direction of the triangular structure and the $\langle 10 \rangle$ direction of the HOPG substrate and found $\theta \approx 26^{\circ}$. In the supplementary information (section 2, figure S3) we use analytic formulae [15] to calculate the MP period, λ , and MP angle, δ , for an Sb₂O₃ layer on HOPG, for a range of Sb₂O₃ lattice constants and twist angles. The best match with experiment is obtained for a lattice constant of 796 pm for Sb_2O_3 and $\theta = 27.6^{\circ}$ and we find that very small deviations (beyond ± 7 pm, and/or $\pm 0.5^{\circ}$) lead to noticeably different MPs which are incompatible with the experimental observations. This result is in almost perfect agreement with the values obtained from atomically resolved imaging of the triangular structures as well as the literature value (789 pm) for $Sb_2O_3(111)$.

We simulated the MP using these parameters and figure 2(b) shows that the overall appearance, period, and alignment of the MP are clearly in very good agreement with the experimental results (figure 2(a)). The relative alignment of the unit cells is schematically shown in figures 2(c) and (d) shows the detailed superposition of the full atomic structures.

All in all our MP analysis strongly supports the conclusion that the triangular structures are formed from Sb₂O₃.

3.3. Spectroscopy results

Initial tunneling spectra of the triangular structures, on both HOPG and Bi islands, were limited to the voltage range between +1 V and -1 V because of the fragility of the islands at high biases. As shown in supplementary figure S4, these spectra were found to be barely distinguishable from those of the substrates. With optimised tips and tunneling conditions it was sometimes possible to obtain spectra in a wider bias range. Figures 3(a), (b) shows the spectra of a triangular structure and the supporting bismuth island (inset in figure 3(a)) obtained between +2 V and -2 V. The local density of states (LDOS) of the triangular structure is almost zero for most of the bias voltage range but grows strongly at high positive voltages. While the spectra from the triangular structure and Bi island in figure 3(a) differ significantly, they do exhibit some common features. Figure 3(b) shows the data in the grey-shaded area in figure 3(a) on a magnified vertical scale, making it clear that two peaks (at $\sim 0.3 \text{ V}$ and $\sim 0.8 \text{ V}$) from the Bi island are found to be weakly present in the spectrum from the triangular structure.

These findings are a manifestation of a gap in the electronic density of states (DOS), as observed for other ultrathin insulating materials [26]. The strong peak in figure 3(a), (b) marks the onset of the conduction band below which there is a wide gap of at least 3.5 eV. Peaks in the substrate DOS are weakly transmitted through or injected into the (effectively insulating) triangular structure [27]. We were unable to detect the valence band onset at negative bias voltage due to the fragility of the islands at high biases.

3.4. Band structure calculations

Since the nanostructures exhibit a triangular symmetry and are atomically thin, it is important to consider the possibility that they are formed of pure Sb. As discussed in the supplementary information, we considered $\beta\text{-Sb}$ itself and two plausible pure Sb structures that have unit cells comparable to that observed in figure 1: a 2×2 reconstruction of the $\beta\text{-}$ antimonene structure with one vacancy per unit cell, and a structure composed of vdW-bonded Sb4 molecules. Supplementary figures S5 and S6 show that the calculated band structures for these structures are clearly inconsistent with the tunneling spectra and can therefore be discarded as potential explanations.

Figures 3(c), (d) shows the calculated band structure and electronic DOS for a single free-standing ML of α -Sb₂O₃(111), while figure 3(e), (f) show corresponding calculations for bulk α -Sb₂O₃(111). The band structure for the ML structure shows a clear indirect band gap of 3.3 eV around the Fermi energy. The calculated band gap is slightly larger than that of the bulk (3.1 eV), as expected. The calculated values are similar to previously reported values for thin film [14] and bulk [6, 7, 28] Sb₂O₃. Overall, the band

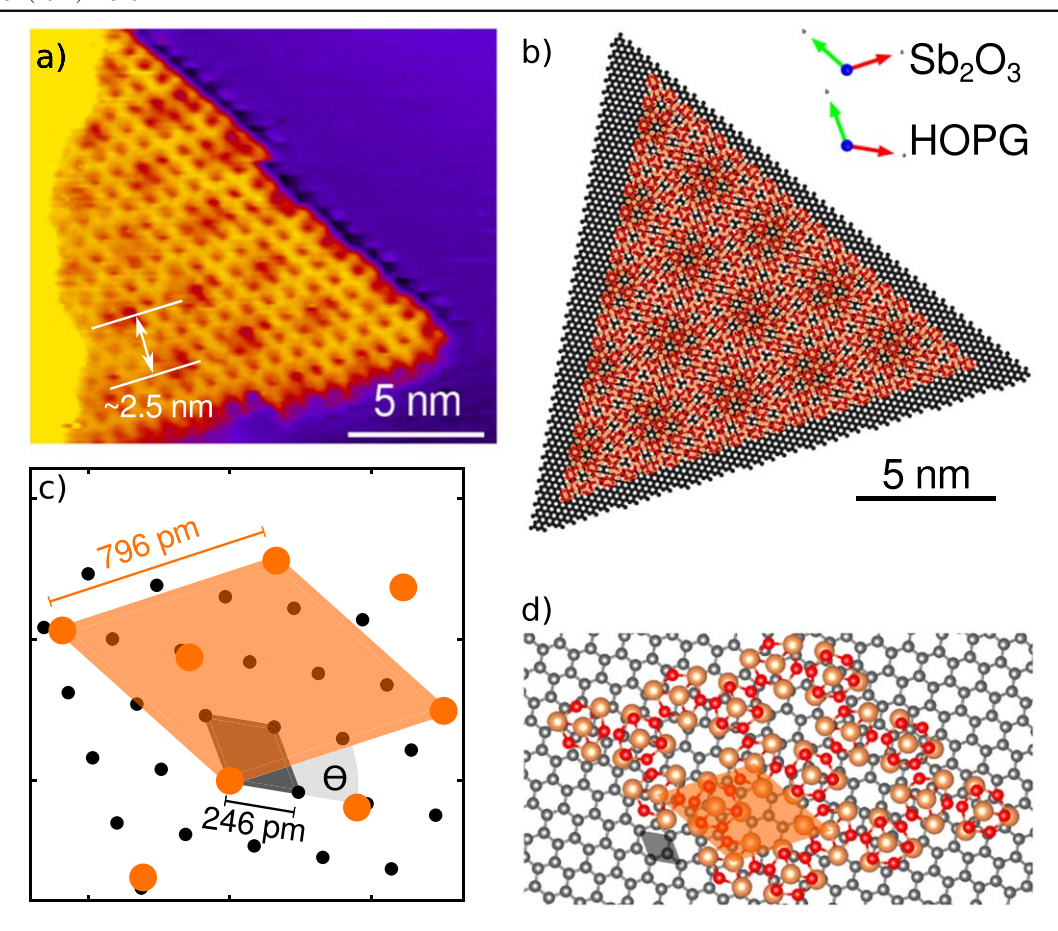


Figure 2. Moiré pattern of triangular structures on HOPG: (a) topography (1 V, 20 pA) of a triangular structure on HOPG, attached to a Bi island on the left. The MP period is indicated in white. (b)-(d) Simulation of the MP of Sb₂O₃ (orange/red layer) on HOPG (grey/black), using lattice constants of 246 pm for HOPG, 796 pm for Sb₂O₃, and a twist angle of $\theta = 27.6^{\circ}$ (see (c)). A global rotation of -9.5° was applied to match the experimental data. (b) Overview of the emerging MP, the scale in (a), (b) is the same. Two labeled coordinate systems show the orientations of the two layers. (c) Schematic view (field of view: $(1.53 \text{ nm})^2$) of the abstract Sb₂O₃ lattice and unit cell (orange) on HOPG (black). The orange circles indicate the positions of Sb_4O_6 molecules, the black spots merely show one HOPG lattice point each. The light grey area indicates the twist angle θ between the two layers. (d) Close-up view (width \times height: 4 nm \times 2.14 nm) of the full structure of the two lattices. A unit cell of each layer is indicated (orange for Sb₂O₃, grey for HOPG).

structure calculations for monolayer Sb₂O₃ are consistent

with the experimental results from the triangular structures.

4. Discussion

4.1. The triangular structures are monolayers of α -Sb₂O₃

The results presented above are all consistent with the conclusion that the triangular structures are monolayers of α-Sb₂O₃. The morphology of the observed triangular structures clearly points to an atomically thin, crystalline material with triangular symmetry. More particularly the large lattice constant of $796 \,\mathrm{pm} \pm 7 \,\mathrm{pm}$ (obtained via analysis of the observed MPs) is compatible with that of α -Sb₂O₃(111). Since the atomic period is independent of the bias voltage and since there is strong evidence for a band gap, we can exclude possible alternative explanations of the long period patterns such as charge density waves. Moreover, the fragility of the triangular structures suggests relatively weak bonding (compared to previously observed 2-dimensional materials such as β -antimonene [19]), as expected for vdW bonds. The bandstructure calculations agree well with the experimental observations and therefore support the conclusion that the triangular structures are monolayers of α -Sb₂O₃.

4.2. Source of the oxide

We now comment on the source of the Sb₂O₃, which is not obvious because the source material is high-purity antimony. Due to the low partial pressure of oxygen under UHV conditions, as well as the known slow oxidation of Sb [29, 30], we exclude the formation of Sb₂O₃ via oxidation of elemental Sb layers as in [31, 32]. Furthermore Sb₂O₃ forms in significant quantities from the metal only at elevated temperatures [13, 29], which suggests that oxidation of the diffusing Sb after deposition is unlikely. This is further supported by the fact that chemical aging of previously observed Sb [19] and Bi [21, 33] structures has so far never been observed in our UHV experiments. We believe instead that small quantities of Sb₂O₃ are formed in the crucible when the UHV chamber is vented for maintenance, and are later re-evaporated (and then deposited) simultaneously with the Sb.

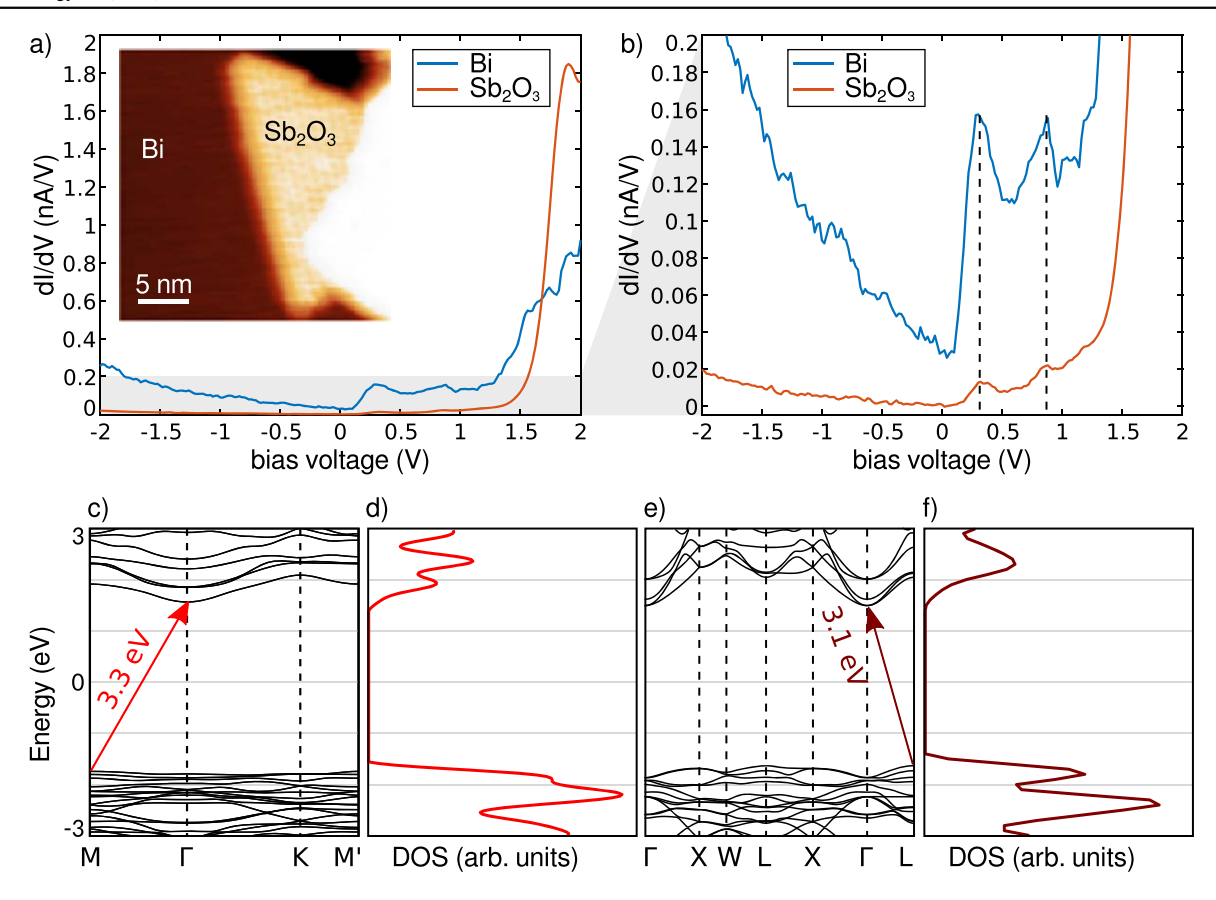


Figure 3. Experimental scanning tunneling spectroscopy data and Sb_2O_3 band structure calculations: (a) spectra from a triangular structure (orange line) and the underlying Bi structure (blue line). Inset shows a topography image of the Sb_2O_3 structure. (b) Magnification of the low-intensity region marked by the grey-shaded bar in (a). Dashed black lines indicate characteristic features of the Bi structure, which are also observed through the insulating Sb_2O_3 . (c) Calculated band structure and (d) DOS for a monolayer of α - Sb_2O_3 (111). The red arrow in (c) marks the electronic band gap of 3.3 eV. (e), (f) Calculated band structure and DOS for bulk Sb_2O_3 for comparison.

Deposition of Sb_2O_3 is facilitated by the much higher vapor pressure of α - Sb_2O_3 compared to elemental Sb^7 .

4.3. Growth

One of the most remarkable aspects of the growth of the α -Sb₂O₃ triangles is that they are formed simultaneously with the growth of pure Sb structures, i.e. layers of α -Sb and β -Sb. All three materials are observed to exist as relatively homogenous films, with minimal defects and no obvious mixed phases or phase boundaries. Since all films are formed through diffusion and aggregation processes [19, 33] these observations suggest that Sb₄O₆ and Sb clusters, which diffuse on the surface simultaneously (see figure 1(e)), aggregate only with other clusters of the same type. We speculate that pairs of Sb₄O₆ clusters are captured at defects on the edges of Bi structures and then allow other Sb₄O₆ clusters to bond and therefore nucleate the formation of triangular structures, whilst elsewhere pairs of Sb clusters can also bond and nucleate pure Sb structures (and then restructure into either the α -Sb or β -Sb phase depending on the local density of the clusters and their arrival rate at the growing structure). The

triangular and pure Sb structures grow by addition of further $\mathrm{Sb_4O_6}$ and $\mathrm{Sb_4}$ clusters. This scenario is based on the hypotheses that bonding is favoured between *like* clusters and that the interaction between $\mathrm{Sb_4}$ and $\mathrm{Sb_4O_6}$ clusters is weak, preventing formation of mixed structures. Obviously it would be interesting to test this speculation using calculations of the binding between the $\mathrm{Sb_4}\text{-}\mathrm{Sb_4}$, $\mathrm{Sb_4O_6}\text{-}\mathrm{Sb_4O_6}$ and $\mathrm{Sb_4}\text{-}\mathrm{Sb_4O_6}$ cluster pairs.

Finally, we note an interesting 'filtering effect' that takes place during growth at the Bi edges. The vast majority of $\mathrm{Sb_2O_3}$ is found on the HOPG substrate at the edges of Bi islands. Few triangular structures were observed on top of the Bi islands, suggesting that they are formed from $\mathrm{Sb_4O_6}$ molecules that directly impinge on the different thickness islands (see schematic in figure 1(e)). This in turn suggests that $\mathrm{Sb_4O_6}$ molecules cannot overcome any Bi edges in significant quantities i.e. that the Ehrlich–Schwoebel (ES) barrier is high. In contrast, pure antimony structures are exclusively found on the Bi islands. Thus we infer that elemental Sb is easily able to climb up over the edges of the islands, i.e. the ES barrier is low. Hence the Bi edges seems to effectively filter the diffusing Sb and $\mathrm{Sb_4O_6}$ material.

 $^{^7}$ At \sim 480 °C, which is the lowest temperature for which experimental values are available for both substances, the vapor pressure of Sb₂O₃ is \sim 35 times that of elemental Sb [34, 35]

5. Conclusions

We have demonstrated controlled growth of single monolayer structures of Sb₂O₃, and that structures which are entirely composed of the α -phase can be achieved without the use of a passivator [5]. Our results suggest the growth of monolayers of Sb₂O₃ might be achievable by direct evaporation of solid Sb₂O₃ from a Knudsen cell. It will be important to explore the growth mode for Sb₂O₃ in the absence of Bi islands, which are important in the present work in providing nucleation sites, and especially whether it is possible to achieve growth of large areas of the monolayer structure. We emphasise that growth of Sb₂O₃ was not observed in previous experiments on HOPG [24] because the observed morphology was dominated by growth of large 3D Sb islands. In the present experiments, the Bi islands appear to play a useful additional role in separating clusters of the two materials (Sb and Sb₂O₃) at the Bi edges, due to their different ES barriers.

Acknowledgments

This work was supported by the MacDiarmid Institute for Advanced Materials and Nanotechnology and the Marsden Fund (UOC1503). XW was supported by the National Natural Science Foundation of China (11204133) and the Jiangsu Province Natural Science Foundation of China (BK2012393). PJK acknowledges support of National Science Centre, Poland (2015/17/B/ST3/02362 and 2019/35/B/ST5/03956) TCC was supported by the US National Science Foundation (DMR-17-09945). GB was supported by the US National Science Foundation (DMR-1809160).

ORCID iDs

Tobias Märkl https://orcid.org/0000-0002-4206-5086

Maxime Le Ster https://orcid.org/0000-0002-3874-799X

Pawel J Kowalczyk https://orcid.org/0000-0001-6310-4366

Simon A Brown https://orcid.org/0000-0002-6041-4331

References

- Akinwande D et al 2019 Graphene and two-dimensional materials for silicon technology Nature 573 507–18
- [2] Deng D, Novoselov K, Fu Q, Zheng N, Tian Z and Bao X 2016 Catalysis with two-dimensional materials and their heterostructures *Nat. Nanotechnol.* 11 218
- [3] Kang S et al 2020 2D semiconducting materials for electronic and optoelectronic applications: potential and challenge 2D Mater. 7 022003
- [4] Geim A K and Grigorieva I V 2013 Van der Waals heterostructures Nature 499 419–25
- [5] Han W et al 2019 Two-dimensional inorganic molecular crystals Nat. Commun. 10 1–10
- [6] Matsumoto A, Koyama Y, Togo A, Choi M and Tanaka I 2011 Electronic structures of dynamically stable As₂O₃, Sb₂O₃, and Bi₂O₃ crystal polymorphs *Phys. Rev.* B 83 214110

- [7] Allen J P, Carey J J, Walsh A, Scanlon D O and Watson G W 2013 Electronic structures of antimony oxides *J. Phys. Chem.* C 117 14759–69
- [8] Tigau N, Ciupina V and Prodan G 2005 The effect of substrate temperature on the optical properties of polycrystalline Sb₂O₃ thin films J. Cryst. Growth 277 529–35
- [9] Tigau N, Ciupina V and Prodan G 2006 Structural, optical and electrical properties of Sb₂O₃ thin films with different thickness J. Optoelectron. Adv. Mater. 8 37–42
- [10] Svensson C 1975 Refinement of the crystal structure of cubic antimony trioxide Acta Crystallogr. B 31 2016–8
- [11] Wu Q et al 2019 Two-dimensional semiconducting and singlecrystalline antimony trioxide directly-grown on monolayer graphene Chem. Commun. 55 2473–6
- [12] Sun G et al 2019 Selective growth of wide band gap atomically thin Sb₂O₃ inorganic molecular crystal on WS2 Nano Res. 12 2781-7
- [13] Yasir M *et al* 2015 Synthesis and properties of crystalline thin film of antimony trioxide on the Si(1 0 0) substrate *Appl. Surf. Sci.* **349** 259–63
- [14] Xiao M et al 2020 Symmetry-reduction enhanced polarizationsensitive photodetection in core-shell SbI3/Sb₂O₃ van der Waals heterostructure Small 16 1907172
- [15] Le Ster M, Maerkl T, Kowalczyk P J and Brown S A 2019 Moiré patterns in van der Waals heterostructures *Phys. Rev.* B 99 1–10
- [16] Le Ster M, Märkl T and Brown S A 2019 Moiré patterns: a simple analytical model 2D Mater. 7 011005
- [17] Momma K and Izumi F 2011 VESTA3 for three-dimensional visualization of crystal, volumetric and morphology data J. Appl. Crystallogr. 44 1272–6
- [18] Kresse G and Furthmüller J 1996 Efficient iterative schemes for ab initio total-energy calculations using a plane-wave basis set *Phys. Rev.* B 54 11169
- [19] Märkl T et al 2018 Engineering multiple topological phases in nanoscale Van der Waals heterostructures: Realisation of α -antimonene 2D Mater. **5** 011002
- [20] Scott S A, Kral M V and Brown S A 2005 A crystallographic orientation transition and early stage growth characteristics of thin Bi films on HOPG Surf. Sci. 587 175–84
- [21] Kowalczyk P J, Mahapatra O, Brown S A, Bian G, Wang X and Chiang T C C 2013 Electronic size effects in three-dimensional nanostructures *Nano Lett.* 13 43–7
- [22] Lu Y et al 2015 Topological properties determined by atomic buckling in self-assembled ultrathin Bi(110) Nano Lett. 15 80-7
- [23] Kowalczyk P *et al* 2020 Realization of symmetry-enforced two-dimensional dirac fermions in nonsymmorphic α -Bismuthene *ACS Nano* 14 1888
- [24] Scott S A and Brown S A 2006 3D growth characteristics of antimony aggregates on graphite Eur. Phys. J. D 39 433
- [25] Kowalczyk P J et al 2017 Single atomic layer allotrope of bismuth with rectangular symmetry Phys. Rev. B 96 205434
- [26] Schintke S and Schneider W D 2004 Insulators at the ultrathin limit: electronic structure studied by scanning tunnelling microscopy and scanning tunnelling spectroscopy *J. Phys.:* Condens. Matter 16 R49–81
- [27] Pan M et al 2016 Modification of the electronic properties of hexagonal boron-nitride in BN/graphene vertical heterostructures 2D Mater. 3 1–8
- [28] Carey J J, Allen J P, Scanlon D O and Watson G W 2014 The electronic structure of the antimony chalcogenide series: Prospects for optoelectronic applications *J. Solid State Chem.* 213 116–25
- [29] Greenwood N N and Earnshaw A (ed) 1997 Chemistry of the Elements (Arsenic, Antimony and Bismuth) 2nd ed (Oxford: Butterworth-Heinemann) ch 13
- [30] Rosenberg A J, Menna A A and Turnbull T P 1960 Kinetics of the oxidation of antimony *J. Electrochem. Soc.* **107** 196

- [31] Wolff S, Gillen R, Assebban M, Abellán G and Maultzsch J 2019 Two-dimensional antimony oxide *Phys. Rev. Lett.* 124 126101
- [32] Assebban M et al 2020 Unveiling the oxidation behavior of liquid-phase exfoliated antimony nanosheets 2D Mater. 7 025039
- [33] Scott S A, Kral M V and Brown S A 2006 Bi on graphite: morphology and growth characteristics of star-shaped dendrites *Phys. Rev.* B 73 1–7
- [34] Hincke W B 1930 The vapor pressure of antimony trioxide *J. Am. Chem. Soc.* **52** 3869–77
- [35] Rosenblatt G M and Ernest Birchenall C 1961 Vapor pressure of antimony by the torsion-effusion method *J. Chem. Phys.* 35 788–94